Available online at www.sciencedirect.com
ScienceDirect
Journal of Catalysis 253 (2008) 253–260
JOURNAL OF CATALYSIS
www.elsevier.com/locate/jcat

# Catalytic oxidation of CO over ordered mesoporous platinum

Ali Saramat [a,b,*], Peter Thormählen [a,c], Magnus Skoglundh [a,b], George S. Attard [d], Anders E.C. Palmqvist [a,b,*]

[a] *Competence Centre for Catalysis, Chalmers University of Technology, SE-412 96 Göteborg, Sweden*
[b] *Applied Surface Chemistry, Department of Chemical and Biological Engineering, Chalmers University of Technology, SE-412 96 Göteborg, Sweden*
[c] *Chemical Physics, Department of Applied Physics, Chalmers University of Technology, SE-412 96 Göteborg, Sweden*
[d] *Department of Chemistry, University of Southampton, Southampton SO17 1BJ, UK*

Received 2 April 2007; revised 8 November 2007; accepted 11 November 2007

**Abstract**

Hexagonal phase mesoporous ($H_1$–Pt) was recently reported to have different catalytic properties compared to conventional platinum catalysts. To further investigate this observation the catalytic activity of $H_1$–Pt/$Al_2O_3$ for CO oxidation was compared with the activity of a corresponding catalyst prepared from Pt-black (Pt-black/$Al_2O_3$). The $H_1$–Pt/$Al_2O_3$ catalyst showed ignition at lower temperatures but extinction at higher temperatures compared to Pt-black/$Al_2O_3$. These observations were further supported by oxygen step-response experiments at constant temperature, where the $H_1$–Pt/$Al_2O_3$ catalyst showed ignition at lower oxygen concentrations when starting from a CO poisoned surface and extinction at higher $O_2$ concentrations when starting from the high-reactive state. Furthermore, adsorption of CO on the catalysts was studied *in situ* using infrared spectroscopy in absence and presence of oxygen after pre-oxidation and pre-reduction, respectively. At 150 °C the $H_1$–Pt/$Al_2O_3$ sample showed activity for CO oxidation in the presence of oxygen regardless of pretreatment, whereas Pt-black/$Al_2O_3$ was inactive due to CO self-poisoning. The differences observed in the low reactive state are suggested to be due to structural differences of the platinum surface in the catalysts resulting in a lower sensitivity of the $H_1$–Pt/$Al_2O_3$ catalyst towards CO self-poisoning and a higher capacity to activate oxygen, and thus a higher activity for CO oxidation. During the high reactive state, the observed higher sensitivity to the concentration ratio between CO and oxygen, and to the temperature is likely due to less optimal ratio between the sticking coefficients of the reactants on the $H_1$–Pt catalyst and to higher mass-transport limitations in its narrower pores during the initial stage of the extinction.


*Keywords:* Platinum; Pt/$Al_2O_3$; Catalyst; CO oxidation; Ignition; Extinction

## 1. Introduction

One of the most commonly used catalysts today is Pt/$Al_2O_3$ which consists of platinum particles supported on alumina. This type of catalyst is used to oxidize, e.g., volatile organic compounds in the exhausts from process industries, and hydrocarbons and CO in exhaust gases from diesel engines. The noble metal is typically present as small crystallites or clusters dispersed on the alumina surface providing a high active surface area and thus effective use of the expensive precious metal. These deposited platinum particles are typically a few nanometers in size and adopt a convex or possibly faceted surface.

Templated synthesis methods using self-organizing media such as lyotropic liquid crystals can be used to prepare ordered mesostructured materials. In 1997 Attard et al. reported that ordered mesoporous platinum could be prepared by chemical reduction of hexachloroplatinic acid (HCPA) in the presence of a liquid crystalline template [1]. Additionally, it was shown that these liquid crystal phases could be used to electrodeposit platinum films containing an ordered mesoporous structure [2–4]. Recently, Yamauchi et al. have shown that the choice of reducing agent is highly significant for the formation of the mesoporous network [5]. Accordingly, the nucleation process and hence the choice of reducing agent is crucial in soft templating synthesis of long-range ordered mesoporous platinum.

* Corresponding authors. Fax: +46 31 16 00 62.
*E-mail addresses:* saramat@chalmers.se (A. Saramat), adde@chalmers.se (A.E.C. Palmqvist).

0021-9517/$ – see front matter 
doi:10.1016/j.jcat.2007.11.007

In contrast to conventional platinum nanoparticles, mesoporous platinum may thus contain an ordered arrangement of pores throughout the structure. Although, the ordered mesoporous platinum particles may have convex perimeter surfaces, the internal pore surface can be prepared such that it is mainly concave [5]. For structure sensitive reactions, in heterogeneous catalysis, the activity and/or selectivity vary with the surface structure of the active phase [6]. It is thus of interest to compare the catalytic performance of an ordered mesoporous hexagonal platinum phase ($H_1$–Pt) to that of conventional Pt nanoparticles. An interesting reaction for such an evaluation is the important CO oxidation reaction, which is known to be structure sensitive at low CO concentrations [6–14]. Recently, we reported that mesoporous $H_1$–Pt/$Al_2O_3$ exhibits different catalytic properties compared to more conventionally prepared Pt/$Al_2O_3$ catalysts [15]. Here, we further evaluate the catalytic and structural properties of the $H_1$–Pt/$Al_2O_3$ catalyst thus highlighting the differences between mesoporous and conventionally prepared platinum. The structure of the two platinum samples was analyzed using TEM, SEM-EDX, wide- and low-angle XRD and $N_2$ physisorption. In addition, the influence of pre-treatment on the catalytic properties of the two different types of platinum was evaluated using oxygen step-response experiments and *in situ* diffuse reflectance infrared Fourier transform spectroscopy (DRIFT).

## 2. Experimental methods

### 2.1. Preparation and characterization of hexagonal mesoporous ($H_1$)-platinum

Ordered mesoporous platinum was prepared following the procedure described by Attard et al. [1]. A mixture containing 4.50 g nonionic surfactant Brij76 (Aldrich), 1.50 g hexachloroplatinic acid, HCPA (Aldrich), and 1.42 g $H_2O$ was prepared forming the $H_1$ liquid crystalline phase, as confirmed using polarized light microscopy. After formation of the crystalline phase, the HCPA was reduced to metallic Pt using a thin sheet of steel. A thin layer of the mixture was thus spread onto a glass tile and the steel sheet was placed on top of the layer and gently pressed down. Reduction of HCPA proceeded at the interface between the mixture and the steel sheet and progressed successively through the mixture. The reduction of HCPA to metallic platinum by iron was complete within 2 h at 40 °C. The solid product was scraped off from the steel sheet and treated with acetone, distilled water, 6 M hydrochloric acid, distilled water, and finally acetone. Using this approach it was possible to maximize the exposed surface area to the steel sheet while still removing unreacted species after completed reduction of HCPA [1]. Finally, the product was characterized by TEM (JEOL, JEM-1200 EX II), SEM-EDX (Leo Ultra 55 FEG), wide-angle XRD (Siemens D5000 X-ray powder diffractometer) and low-angle XRD (Bruker AXS D8 Advance X-ray powder diffractometer). The diffractometers used Cu$K_\alpha$ radiation ($\lambda = 1.542$ Å) as X-ray source. Moreover, nitrogen sorption isotherms were measured on degassed samples at −196 °C with a TriStar 3000 instrument (Micrometrics) to allow for the calculation of the specific surface area according to the BET method [16], and the pore-size distribution according to the BJH method [17]. High surface area platinum (Pt-black, Alfa Aesar, item No. 43838) was used as received.

Table 1
Characteristics of the Pt-catalysts determined by EDX and $N_2$ adsorption/desorption

| Catalyst | Pt/Al/O (wt%) | Pt-loading (mg) | Pt surface area ($m^2/g$) |
|---|---|---|---|
| $H_1$–Pt | 28/30/42 | 0.50 | 34.9 |
| Pt-black | 22/34/44 | 0.39 | 34.2 |

### 2.2. Catalyst preparation

The catalyst samples were prepared using a ferritic chromium steel substrate (C = 0.02%, Cr = 20%, Al = 5.5%, rare earth elements = 0.02% and balance Fe, Sandvik 0C404, Sandvik) with a thickness of 0.03 mm, that is commercially used as substrate in three-way catalysts. The substrate was shaped as circular discs with a diameter of 7 mm (surface area of 38.5 $mm^2$). The discs were pretreated with acetone and subsequently calcined in air at 1000 °C for 24 h, which ensured formation of an oxide surface enabling good adhesion between substrate and support. A slurry of alumina was prepared from 8.0 g $\gamma$-$Al_2O_3$ (Puralox SBa 200, Sasol Germany GmbH), 2.0 g boehmite (Disperal S, Sasol Germany GmbH), 30 mg polyacrylic acid (Dolapix PC21), 67.5 g distilled water and 22.5 g ethanol (+99.5%, Kemetyl). For each Pt sample ($H_1$–Pt and Pt-black) 5.0 g of the alumina slurry was mixed with 0.15 g Pt and subsequently ultrasonicated for 10 min. The slurry was deposited on the calcined substrate using an air-brush in an amount corresponding to approximately 2.0 mg of the final support. The air-brush nozzle pressure was 2 bar and the catalyst substrate was fixed on a magnetic heater with the temperature of the heater set to 200 °C. The catalyst samples were finally calcined in air at 250 °C for 30 min. The elemental composition of each catalyst was determined using SEM-EDX, see Table 1.

### 2.3. Catalytic evaluation

The ignition and extinction processes for CO oxidation were followed as functions of temperature and the $\beta$-value, defined as $\beta = p_{CO}/(p_{CO} + p_{O_2})$, respectively. Due to the low amount of catalytic material available a suitable reactor system for activity measurements of the prepared catalysts was used [18]. The oxidation of CO was studied within the temperature range of 100–250 °C. The catalysts were pretreated in a net-oxidizing feed that consisted of 20 vol% $O_2$ balanced with Ar (carrier gas) in which the samples were heated to 250 °C with a heating rate of 20 °C/min. Subsequently, the temperature was decreased to 25 °C with a cooling rate of 20 °C/min. Following pre-treatment, the ignition and extinction profiles for the catalyst samples were measured in a feed stream consisting of 2000 vol ppm CO, 20 vol% $O_2$ and balanced with Ar. The gas flow rate was 20 ml/min. The heating/cooling rate was 8 °C/min and a dwell time of 2 min at the maximum temperature 250 °C was employed. The outlet gas composition was

analyzed using a mass spectrometer (Balzer QMA 120) where the $m/e$ ratios 2, 28, 32, 40 and 44 were measured and used to calculate the concentrations of $H_2$, CO, $O_2$, Ar and $CO_2$, respectively.

Following analysis of the CO conversion as function of temperature, the low-temperature catalytic activity was further studied as function of the $\beta$-value at constant temperature using the same reactor set-up. At each temperature the oxygen concentration was stepwise increased from 0 to 20 vol% (i.e. $\beta = 1$–$0.01$). Before stepwise decreasing the oxygen concentration in the reverse order, from 20 to 0 vol%, the temperature was intermittently increased to 250 °C for 10 min and then lowered to the initial value. Three different temperatures were studied (150, 160 and 170 °C) and the outlet concentrations of CO and $CO_2$ were recorded at steady-state after a reaction time of 10 min, at each condition studied. At each temperature the catalysts were pretreated in the net-oxidizing feed described above.

### 2.4. In situ DRIFT analysis

The formation of adsorbates on the $H_1$–Pt/$Al_2O_3$ and Pt-black/$Al_2O_3$ samples was followed *in situ* by FTIR spectroscopy in diffuse reflectance mode with a BioRad FTS6000 spectrometer equipped with a Harrick Praying Mantis DRIFT cell [19]. Before spectra were taken, the samples were pre-oxidized *in situ* (20 vol% $O_2$ in Ar at 250 °C for 10 min). Background spectra were collected at 150 °C in Ar. The samples were subsequently saturated with CO in a 2000 vol ppm CO flow (without oxygen present). Then, the samples were exposed to a CO/$O_2$ mixture (2000 vol ppm CO, 20 vol% $O_2$ balanced with Ar, $\beta = 0.01$) at a total gas flow of 200 ml/min (NTP), while the temperature was kept constant at 150 °C. At steady-state conditions (after approximately 10 min) a single spectrum was recorded for each gas mixture. The procedure was repeated for the pre-reduced samples (5 vol% $H_2$ in Ar at 250 °C for 10 min). To illuminate the effect of oxygen introduction the spectra collected in the absence of oxygen were subtracted from the corresponding spectra collected in the presence of oxygen. The outlet gas composition from the DRIFT cell was analyzed using a mass spectrometer (Balzers QMG 422).

## 3. Results and discussion

### 3.1. Characterization of platinum samples

The nitrogen adsorption/desorption isotherms for $H_1$–Pt and Pt-black are shown in Fig. 1. The pore-size distributions for the two samples, calculated from the nitrogen adsorption isotherms [20] are shown in the inset in Fig. 1. The $H_1$–Pt sample shows a narrow pore-size distribution with a mean pore diameter of 3.4 nm, whereas the Pt-black sample shows a broad peak with maximum at a considerably larger diameter, 15 nm. Moreover, the measured BET surface areas are 34.9 and 34.2 $m^2/g$ for $H_1$–Pt and Pt-black, respectively, as shown in Table 1. These results are in good agreement with the previous reports on mesoporous Pt [1,21].

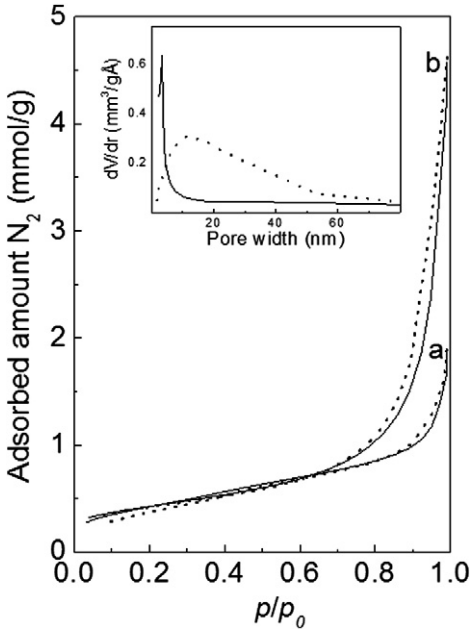


Fig. 1. Nitrogen adsorption (—) and desorption (···) isotherms for (a) $H_1$–Pt and (b) Pt-black powders. Inset shows pore-size distributions for $H_1$–Pt (—) and Pt-black (···) powders calculated from the adsorption isotherms.

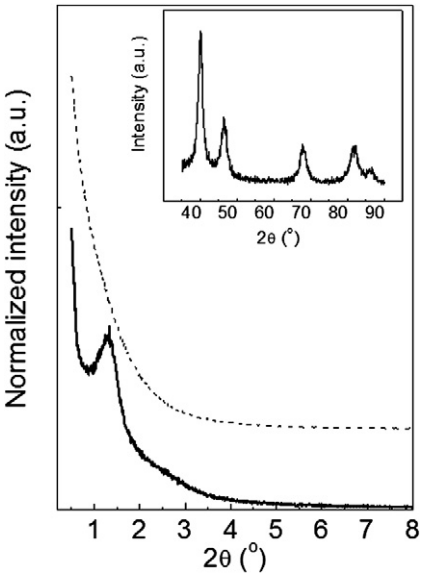


Fig. 2. The low-angle XRD patterns of $H_1$–Pt (—) and Pt-black (···) powders before deposition on $Al_2O_3$. The inset illustrates the wide-angle XRD pattern for the $H_1$–Pt powder.

The low-angle XRD patterns of $H_1$–Pt and Pt-black are shown in Fig. 2. While the Pt-black sample shows no long-range order, the $H_1$–Pt sample shows an ordered mesoporous structure with a peak at $2\theta = 1.4°$ corresponding to a $d_{10}$ spacing of 6.6 nm. For a two-dimensional hexagonal structure the dimension of the unit cell axis, $a$, is related to $d_{10}$ according to the following equation [22]

$$a = \frac{2}{\sqrt{3}} \cdot d_{10}. \tag{1}$$

Accordingly, $a = 7.6$ nm for the $H_1$–Pt sample. Taking into account the pore diameter of 3.4 nm, the wall thickness is cal-

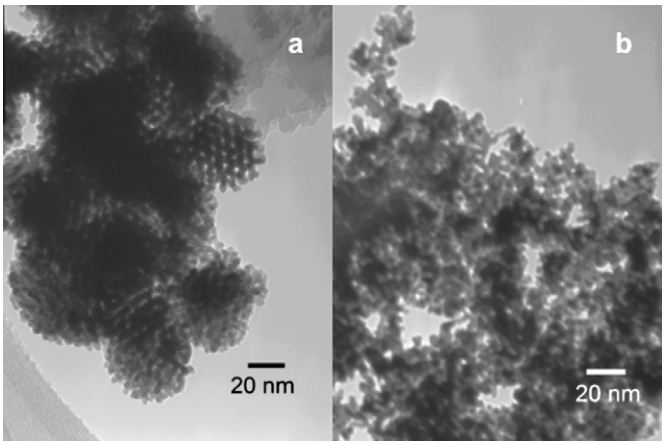


Fig. 3. TEM images of (a) $H_1$–Pt and (b) Pt-black powders shown in a magnification of 300,000.

culated to be 4.2 nm. The wide-angle XRD pattern, inset in Fig. 2, shows that the walls of the $H_1$–Pt sample are crystalline. The TEM micrographs shown in Fig. 3 confirm the presence of hexagonal meso-order in the $H_1$–Pt sample, and the absence of long-range order in the Pt-black sample. We can thus conclude that the synthesis of $H_1$–Pt was successful. As shown by Yamauchi et al. using high resolution TEM, a $H_1$–Pt sample prepared according to a similar preparation route as in the present study, mainly exposes concave platinum surfaces inside the pore structure [5]. The detailed microstructure of the inner surfaces of the pores is not known. It is, however, likely that they predominantly consist of interconnected narrow terraces containing high coordinated terrace sites and inverse step sites with even higher coordination. Thus, the concentration of high coordinated sites is higher in the $H_1$–Pt sample than in a nanoparticulate Pt sample such as Pt-black.

The total amount of deposited support and the overall platinum content were determined by SEM-EDX for each of the prepared catalyst samples. The total platinum content of both samples was within the range 45 mg Pt ±13%, see Table 1.

### 3.2. Evaluation of catalytic performance

In Fig. 4 the oxidation of CO to $CO_2$ over the catalyst samples is shown as a function of temperature. Both samples show sharp ignition profiles and a hysteresis for the corresponding extinction profile. For $H_1$–Pt/$Al_2O_3$ the ignition proceeds at lower temperatures compared to Pt-black/$Al_2O_3$. The turn-over frequency (TOF) expressed as the conversion rate for CO oxidation normalized per Pt surface area was previously found to be about 10 times higher for the $H_1$–Pt/$Al_2O_3$ sample during this stage [15]. Furthermore the Pt-black/$Al_2O_3$ sample shows the widest hysteresis between the ignition and extinction profiles, and also sustained CO oxidation at lowest temperatures during the extinction phase.

For the Pt/$Al_2O_3$ system, recent work on model catalysts have shown higher turn-over frequencies and lower activation energies for CO oxidation over 14 nm Pt particles than over 1.7 nm Pt particles [9]. The suggested explanation for this was changes in the desorption kinetics of CO with particle size [9].

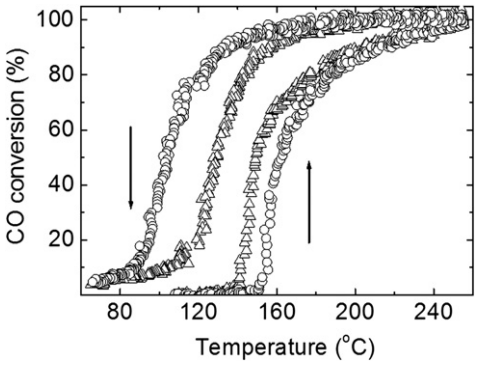


Fig. 4. Catalytic conversion of CO to $CO_2$ over $H_1$–Pt/$Al_2O_3$ (△) and Pt-black/$Al_2O_3$ (○). The heating/cooling rate was 8 °C/min and the dwell time at $T_{max} = 250$ °C was 2 min.

It has, however, been shown that the heat of adsorption of linear CO species on Pt/$Al_2O_3$ is not much affected by the dispersion of Pt suggesting the need for alternative explanations [10]. Furthermore, higher activity for CO oxidation of larger Pt particles supported on silica has been explained by lower concentration of low-coordinated surface sites, like edges and corners on such particles. The reaction rate for CO oxidation over these type of sites has been estimated to be 10 times lower compared to planar surfaces, assigned to that the reactants are more strongly adsorbed at corner and edge sites and thus need to surpass an additional energy barrier to diffuse and react [12]. In addition, no systematic changes of the reaction order of CO with respect to particle size were found, whereas a decrease in the CO oxidation reaction order with respect to the partial pressure of oxygen was found with decreasing Pt particle size [13].

For CO oxidation over Pt/$Al_2O_3$, both experimental studies and theoretical simulations have previously suggested that the sticking coefficient for oxygen varies between the low and high reactive state [23]. During the high reactive state, the Pt surface is likely partially oxidized with different adsorption kinetics compared to the low reactive state [24]. Our observations suggest that the $H_1$–Pt/$Al_2O_3$ sample is less sensitive than Pt-black/$Al_2O_3$ towards self-poisoning by CO during the ignition phase. This can in principle be due to either (i) a more facile desorption of CO from the $H_1$–Pt/$Al_2O_3$ sample, or (ii) a more facile dissociative adsorption of $O_2$ on $H_1$–Pt/$Al_2O_3$. However, for the transition from the high to the low reactive state the $H_1$–Pt/$Al_2O_3$ sample is more sensitive resulting in a higher onset temperature of the extinction phase for $H_1$–Pt/$Al_2O_3$ compared to the Pt-black/$Al_2O_3$ sample. The reason for this is more difficult to asses unambiguously. Most likely kinetics is limiting either through decreased dissociative adsorption of oxygen or increased CO self-poisoning. However, higher mass transport restrictions in the narrower pores of the $H_1$–Pt/$Al_2O_3$ sample may also affect the initial stage of the extinction phase.

In order to further illuminate the differences in ignition and extinction between the two catalysts the effects of step changes in inlet gas composition were studied at constant temperature. In Fig. 5 the CO and $CO_2$ outlet gas concentrations are shown during stepwise decrease and increase of the $\beta$-value. The measurements were performed at three different temperatures (150,

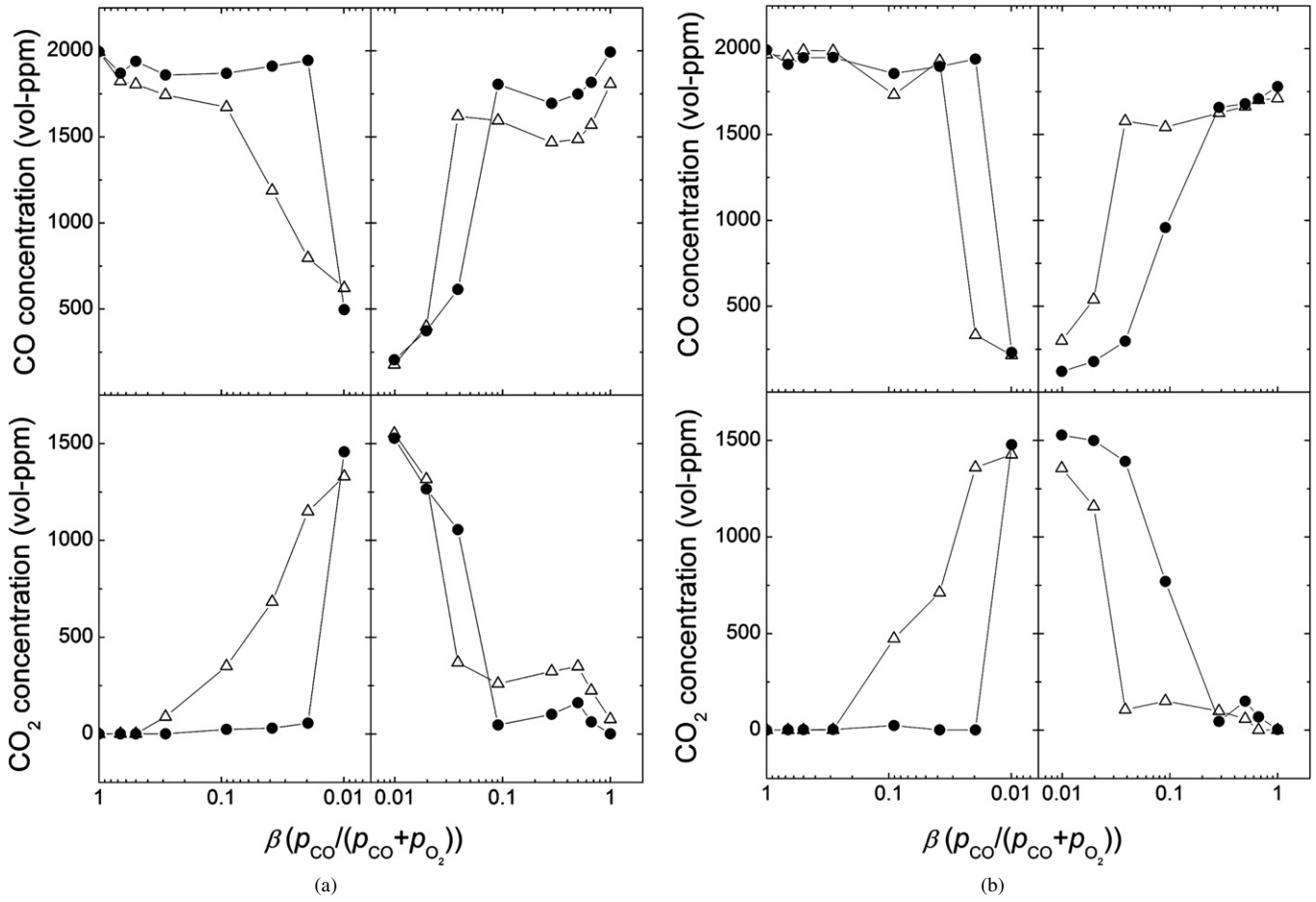


Fig. 5. Concentrations of CO and $CO_2$ at reactor outlet as a function of feed composition expressed as $\beta = p_{CO}/(p_{CO} + p_{O_2})$ over $H_1$–Pt/$Al_2O_3$ (△) and Pt-black/$Al_2O_3$ (●) at (a) 150 °C, (b) 160 °C and (c) 170 °C. [CO] was kept constant at 2000 vol ppm whereas [$O_2$] was varied in the following sequence: 0 vol%, 0.1%, 0.2%, 0.5%, 2%, 5%, 10%, 20% (i.e., $\beta = 1$–0.01), and then in the reverse order from 20% to 0.1% (i.e. $\beta = 0.01$–1). Midway through these [$O_2$] variations, at [$O_2$] = 20%, the temperature was intermittently increased to 250 °C for 10 min to ensure that the catalysts were in the high reactive state.

160 and 170 °C) to cover the most interesting part of the conversion interval in Fig. 4, and are shown in Figs. 5a–5c, respectively. At 150 and 160 °C, the $H_1$–Pt/$Al_2O_3$ sample shows CO conversion at a higher $\beta$-value (i.e., lower $O_2$ concentration) than the Pt-black/$Al_2O_3$ sample during the ignition phase whereas at 170 °C no large differences are found between the samples. At high $\beta$-values the conversion of CO is low and the overall reaction rate is kinetically controlled rather than mass transport limited. During such conditions the reaction is self-poisoned due to strong CO adsorption on platinum. Judging from Fig. 5, the $H_1$–Pt/$Al_2O_3$ sample has a higher capacity to activate oxygen supporting the notion that it has a lower concentration of low coordinated sites [14]. This indicates that the ratio between the sticking coefficients of CO and oxygen is more favorable for the $H_1$–Pt/$Al_2O_3$ sample, which results in lower sensitivity to CO self-poisoning compared to the Pt-black/$Al_2O_3$ sample.

Following the intermediate temperature increase to 250 °C the catalysts are well within the high reactive state. During the subsequent stepwise increase of the $\beta$-value the CO conversion over the $H_1$–Pt/$Al_2O_3$ sample declines faster (at $\beta = 0.04$) compared to Pt-black/$Al_2O_3$. This observation is in agreement with Fig. 4, where the activity for CO oxidation for $H_1$–Pt/$Al_2O_3$ declines faster at higher temperatures than for Pt-black/$Al_2O_3$.

To summarize the results from the evaluation of the catalytic properties, the $H_1$–Pt/$Al_2O_3$ catalyst shows higher activity compared to Pt-black/$Al_2O_3$ during the low reactive state, where the activity is determined by the surface reaction. This is likely due to a lower sensitivity of the $H_1$–Pt/$Al_2O_3$ sample towards CO self-poisoning. However, in the high reactive state the reaction over the $H_1$–Pt/$Al_2O_3$ catalyst is more sensitive to the ratio between CO and oxygen and the temperature compared to Pt-black/$Al_2O_3$. We mainly attribute this to a less optimal ratio between the sticking coefficients for CO and oxygen during the transition from high to low reactive state for the $H_1$–Pt/$Al_2O_3$ sample [25,26].

### 3.3. In situ DRIFT analysis

To further understand the differences in activity between the samples, in situ DRIFT analysis was performed and a comparison between oxidizing and reducing pre-treatment was carried out. The DRIFT spectra of the two samples, shown in Fig. 6 a–d, were collected at 150 °C with either only CO or with both CO and $O_2$ in the feed. Gas phase CO has two absorp-

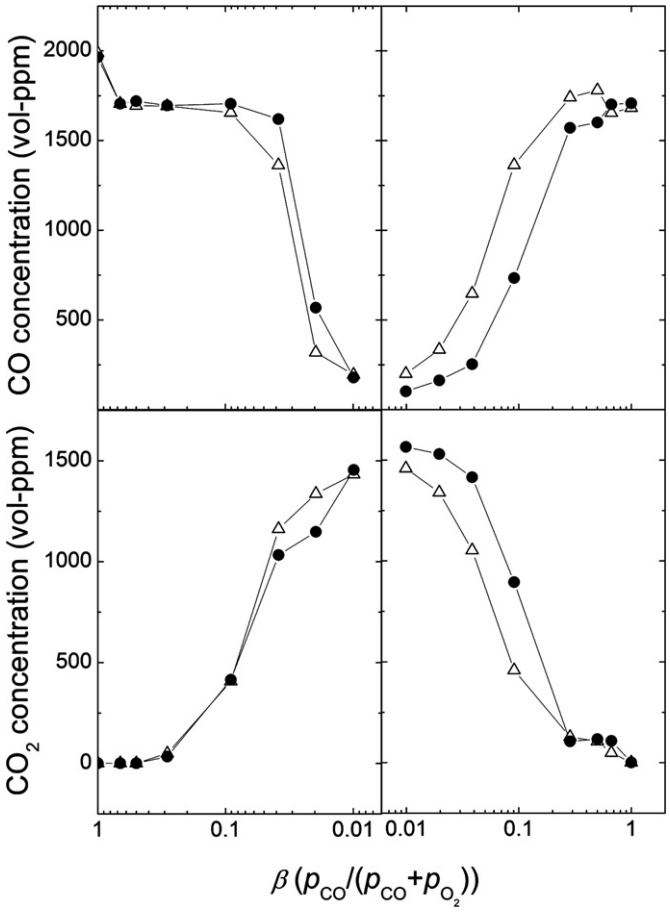


(c)

Fig. 5. (*continued*)

tion branches centered around 2170 and 2110 $cm^{-1}$, respectively, and is the dominating component in Fig. 6 a–d. However, the spectra also contain information of surface adsorbates. For adsorbed CO on Pt, terminal bonded CO has absorption bands between 2090 and 2070 $cm^{-1}$, double bridge-bonded CO at 1850–1750 $cm^{-1}$, and triple bridge-bonded CO at 1730–1620 $cm^{-1}$ [27]. In the present study the adsorbed CO on $H_1$–Pt/$Al_2O_3$ and Pt-black/$Al_2O_3$ seems to be predominantly terminal bonded with an absorption band centered in the interval 2090–2070 $cm^{-1}$, both in the absence and presence of oxygen. The difference spectra in Fig. 6 show differences in the type and amount of CO adsorbed on platinum between exposures for the two different feeds. Consequently, a positive absorption band in the difference spectrum indicates an increase in the amount of adsorbed CO when oxygen is present in the feed. A negative band, on the other hand, specifies a decrease in the amount of adsorbed CO upon introduction of oxygen.

For Pt-black/$Al_2O_3$ (Fig. 6 a and b) the intensity of the band for adsorbed CO at 2095 $cm^{-1}$ is higher for the pre-oxidized than for the pre-reduced sample when only CO is present in the feed. For both pretreatments the intensity of the band for adsorbed CO increases upon introduction of oxygen where the most intense band appears at 2095 $cm^{-1}$ for the pre-oxidized sample and at 2090 $cm^{-1}$ for pre-reduced Pt-black/$Al_2O_3$. This observation is indicative of oxygen promoted CO adsorption.

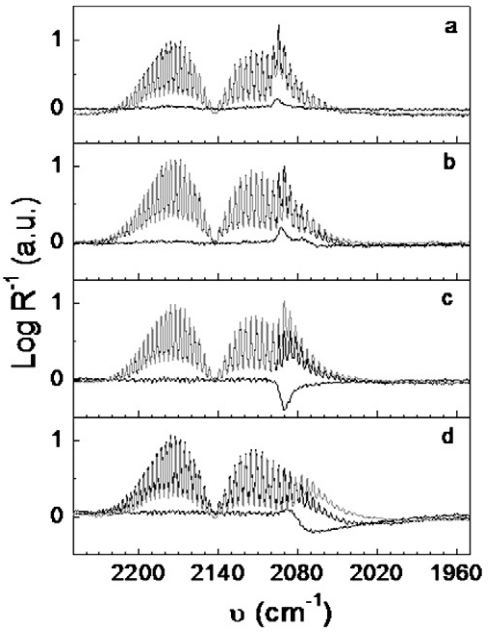


Fig. 6. DRIFT spectra of supported Pt catalysts: (a) pre-oxidized Pt-black/$Al_2O_3$, (b) pre-reduced Pt-black/$Al_2O_3$, (c) pre-oxidized hexagonal mesoporous $H_1$–Pt/$Al_2O_3$ and (d) pre-reduced hexagonal mesoporous $H_1$–Pt/$Al_2O_3$. Gray lines describe the case with only CO in the feed; black lines represent a feed with both CO and $O_2$ and the difference spectra are shown as black solid lines beneath the IR spectra. The frequency interval described on the $x$-axis is typical for adsorbed CO on Pt.

The introduction of oxygen may result in increased adsorption of CO due to either partial oxidation of the platinum surface or by interaction between co-adsorbed CO and oxygen [28]. Absorption bands observed at 2090–2095 $cm^{-1}$ have previously been assigned to linearly adsorbed CO on either metallic Pt sites on large Pt particles or on partially oxidized platinum sites [10,11,29–31].

The difference spectrum for pre-oxidized Pt-black/$Al_2O_3$ in Fig. 6a shows that the largest increase in CO adsorption occurs at sites with absorption centered at 2096 $cm^{-1}$, whereas the corresponding value for the pre-reduced sample is 2093 $cm^{-1}$. In addition, a weak negative band is observed in the difference spectrum of the pre-reduced sample around 2065 $cm^{-1}$, which is attributed to CO adsorbed on metallic platinum [30]. This negative band may be due to: (i) CO oxidation, (ii) CO desorption, or (iii) oxygen-induced change in the adsorption of CO on platinum. The latter may be due to partial oxidation of platinum or co-adsorption of oxygen. Since only minor changes in the mass spectrometer signals for CO and $CO_2$ were observed upon introduction of oxygen (not shown) and a positive absorption band appears at 2093 $cm^{-1}$, we attribute the negative band to an oxygen-induced change of the adsorbed CO on platinum.

In absence of oxygen, there are larger differences in the IR spectra between the pre-reduced and pre-oxidized $H_1$–Pt/$Al_2O_3$ sample (Fig. 6 c and d) compared to Pt-black/$Al_2O_3$ (Fig. 6 a and b). The IR spectrum for $H_1$–Pt/$Al_2O_3$ when only CO is present in the feed shows a strong band at 2090 $cm^{-1}$ for the pre-oxidized case (Fig. 6c) whereas for the pre-reduced sample the absorption band is centered around 2070 $cm^{-1}$ (Fig. 6d). This difference is most probably due to whether or not oxygen

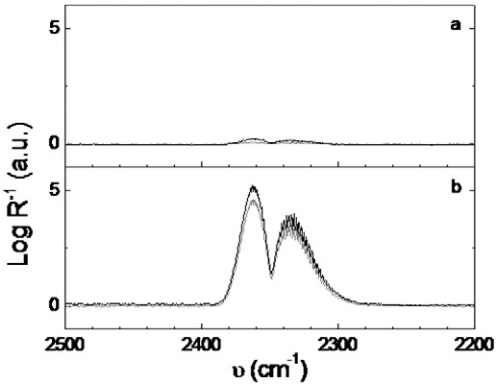


Fig. 7. $CO_2$ (g) peaks in DRIFT spectra in a feed consisting of 2000 vol ppm CO and 20 vol% $O_2$, and balanced with Ar, over (a) Pt-black/$Al_2O_3$ and (b) hexagonal mesoporous $H_1$–Pt/$Al_2O_3$. Gray lines describe the pre-oxidized Pt catalysts and the black lines describe pre-reduced Pt catalysts.

is present on the platinum surface. The absorption band centered at 2070 cm$^{-1}$ is attributed to CO on metallic platinum. On the surface of the pre-oxidized sample, however, accessible oxygen is expected to interact with adsorbed CO, thus causing a shift of the absorption band by about 20 cm$^{-1}$ towards higher wavenumbers.

According to Fig. 6 a and b, regardless of the pretreatment, the Pt-black/$Al_2O_3$ catalyst remains self-poisoned by CO upon introduction of oxygen to the feed. However, the difference spectrum for the pre-oxidized $H_1$–Pt/$Al_2O_3$ sample (Fig. 6c) reveals, that adsorbed CO with the absorption band centered at 2090 cm$^{-1}$, is oxidized to $CO_2$ as the intensity of this band decreases upon introduction of oxygen to the feed. Moreover, the difference spectrum of the pre-reduced $H_1$–Pt/$Al_2O_3$ sample (Fig. 6d), shows a pronounced negative band at 2077 cm$^{-1}$ and a weak positive absorption band at 2090 cm$^{-1}$. In contrast to Pt-black/$Al_2O_3$, the formation of $CO_2$ is confirmed by absorption bands typical for gas phase $CO_2$ at 2360 and 2330 cm$^{-1}$ over both pre-oxidized and pre-reduced $H_1$–Pt/$Al_2O_3$, see Fig. 7.

When considering the $H_1$–Pt/$Al_2O_3$ sample, it seems that the adsorbed CO which is oxidized to $CO_2$ is differently bonded on the pre-reduced sample compared to the pre-oxidized sample (compare the negative bands at 2077 and 2090 cm$^{-1}$ in Fig. 6). However, it is likely that CO adsorbed on the pre-reduced sample (with corresponding band at 2077 cm$^{-1}$) is affected by oxygen and thus causing a shift of the absorption band to 2090 cm$^{-1}$, before reaction to $CO_2$. This would also result in a difference spectrum with a small positive peak at 2090 cm$^{-1}$ and a large negative band at 2077 cm$^{-1}$. Such a rearrangement was observed for the pre-reduced Pt-black/$Al_2O_3$ sample in Fig. 6b, which, however, did not show significant $CO_2$ formation and thus a more pronounced positive peak at 2090 cm$^{-1}$. This alternative interpretation would suggest that the difference in reactivity between the $H_1$–Pt/$Al_2O_3$ and Pt-black/$Al_2O_3$ samples is mainly due to the adsorption of oxygen rather than the presence of specific reactive adsorbed CO species. Thus, the higher sensitivity of $H_1$–Pt/$Al_2O_3$ to pretreatment as well as its higher activity for oxidation of CO may be due to higher ability to activate oxygen on its surface compared to Pt-black/$Al_2O_3$.

To summarize the results from the DRIFT analysis, the reason for the difference in activity for CO oxidation between $H_1$–Pt/$Al_2O_3$ and Pt-black/$Al_2O_3$ is likely due to structural differences of the platinum surfaces, which previously have been shown to affect the adsorption of oxygen by both experimental [32] and theoretical [28] studies. By taking into account the results from the study by Yamauchi et al. [5] it is plausible that the systematic occurrence of high coordinated surface sites such as terrace sites and inverse step sites in the pores of the $H_1$–Pt sample enhances the adsorption of oxygen and thus promotes the $CO_2$ production on platinum in the low reactive state at low temperatures.

## 4. Conclusions

Hexagonal mesoporous $H_1$–Pt, prepared using the method developed by Attard et al. was deposited on $Al_2O_3$ and evaluated as catalyst for CO oxidation in comparison with Pt-black/$Al_2O_3$. The $H_1$–Pt/$Al_2O_3$ catalyst showed ignition at lower temperatures but extinction at higher temperatures compared to Pt-black/$Al_2O_3$. These findings were in agreement with results from oxygen step-response experiments at constant temperature, where the $H_1$–Pt/$Al_2O_3$ catalyst showed ignition at lower oxygen concentrations in the low reactive state and extinction at higher oxygen concentrations in the high reactive state.

This is likely due to lower sensitivity towards CO self-poisoning and a higher capacity to activate oxygen of the $H_1$–Pt/$Al_2O_3$ catalyst in the low reactive state due to structural differences of the platinum surfaces. The $H_1$–Pt/$Al_2O_3$ catalyst with predominantly concave Pt surfaces appears to promote dissociative oxygen adsorption and thus exhibits an enhanced CO oxidation rate at the low reactive state. The higher sensitivity to the concentration ratio between CO and oxygen, and the temperature during the high reactive state may be explained by less optimal ratio between the sticking coefficients for the reactants on the $H_1$–Pt/$Al_2O_3$ sample and higher mass-transport limitations in its narrower pores during the initial stage of the extinction.

## Acknowledgments

This work has been performed at the Competence Centre for Catalysis, which is financially supported by The Swedish Energy Agency, AB Volvo, Volvo Car Corporation, Scania CV AB, GM Powertrain Sweden AB, Haldor Topsøe A/S, and The Swedish Space Corporation. A.E.C.P. thanks the Swedish Research Council for a Senior Researcher grant. M.Sc. Elin Becker at Chalmers University of Technology is thanked for her assistance with the FTIR spectroscopy measurements. Ph.D. Kjell Wikander at Chalmers University of Technology and Professor Karl Wilhelm Törnroos at University of Bergen, are greatly acknowledged for their assistance with the low-angle XRD measurements.

## References


[1] G.S. Attard, J.M. Corker, C.G. Göltner, S. Henke, R.H. Templer, Angew. Chem. Int. Ed. Engl. 36 (1997) 1315.
[2] G.S. Attard, P.N. Bartlett, N.R.B. Coleman, J.M. Elliott, J.R. Owen, Langmuir 14 (1998) 7340.
[3] G.S. Attard, N.R.B. Coleman, J.M. Elliott, Stud. Surf. Sci. Catal. 117 (1998) 89.
[4] G.S. Attard, P.N. Bartlett, N.R.B. Coleman, J.M. Elliott, J.R. Owen, J.H. Wang, Science 278 (1997) 838.
[5] Y. Yamauchi, T. Momma, M. Fuziwara, S.S. Nair, T. Ohsuna, O. Terasaki, T. Osaka, K. Kuroda, Chem. Mater. 17 (2005) 6342.
[6] E. McCarthy, J. Zahradnik, G.C. Kuczynski, J.J. Carberry, J. Catal. 39 (1975) 29.
[7] J.L. Gland, M.R. McClellan, F.R. McFeely, J. Chem. Phys. 79 (1983) 6349.
[8] A. Szabó, M.A. Henderson, J.T. Yates Jr., J. Chem. Phys. 96 (1992) 6191.
[9] G.S. Zafiris, R.J. Gorte, J. Catal. 140 (1993) 418.
[10] A. Bourane, D. Bianchi, J. Catal. 218 (2003) 447.
[11] P.T. Fanson, W.N. Delgass, J. Lauterbach, J. Catal. 204 (2001) 35.
[12] F.J. Gracia, L. Bollmann, E.E. Wolf, J.T. Miller, A.J. Kropf, J. Catal. 220 (2003) 382.
[13] B. Atalik, D. Uner, J. Catal. 241 (2006) 268.
[14] H.D. Lewis, D.J. Burnett, A.M. Gabelnick, D.A. Fischer, J.L. Gland, J. Phys. Chem. B 109 (2005) 21847.
[15] A. Saramat, M. Andersson, S. Hant, P. Thormählen, M. Skoglundh, G.S. Attard, A.E.C. Palmqvist, Eur. Phys. J. D 43 (2007) 209.
[16] S. Brunauer, P.H. Emmett, E. Teller, J. Am. Chem. Soc. 60 (1938) 309.
[17] P.E. Barrett, L.G. Joyner, P.P. Halenda, J. Am. Chem. Soc. 73 (1951) 373.
[18] P. Thormählen, Ph.D. thesis, Chalmers University of Technology, Göteborg, 2001.
[19] J. Jansson, A.E.C. Palmqvist, E. Fridell, M. Skoglundh, L. Österlund, P. Thormählen, V. Langer, J. Catal. 211 (2002) 387.
[20] J.C. Groen, L.A.A. Peffer, J. Pérez-Ramiréz, Microporous Mesoporous Mater. 60 (2003) 1.
[21] B. Gollas, J.M. Elliott, P.N. Bartlett, Electrochim. Acta 45 (2000) 3711.
[22] O. Glatter, O. Kratky, Small Angle X-Ray Scattering, Academic Press, London, 1982.
[23] P.-A. Carlsson, M. Skoglundh, P. Thormählen, B. Andersson, Top. Catal. 30–31 (2004) 375.
[24] L. Österlund, S. Kielbassa, C. Werdinius, B. Kasemo, J. Catal. 215 (2003) 94.
[25] P.-A. Carlsson, M. Skoglundh, E. Fridell, E. Jobson, B. Andersson, Catal. Today 73 (2002) 307.
[26] D. Kulginov, M. Rinnemo, B. Kasemo, J. Phys. Chem. B 103 (1999) 3170.
[27] R.P.H. Gasser, An Introduction to Chemisorption and Catalysis by Metals, Clarendon Press, Oxford, 1985.
[28] A. Alavi, P. Hu, T. Deutsch, P.L. Silvestrelli, J. Hutter, Phys. Rev. Lett. 80 (1998) 3650.
[29] A.Y. Stakheev, E.S. Shpiro, O.P. Tkachenko, N.I. Jaeger, G. Schulz-Ekloff, J. Catal. 169 (1997) 382.
[30] Y. Barshad, X. Zhou, E. Gulari, J. Catal. 94 (1985) 128.
[31] M. Primet, J. Catal. 88 (1984) 273.
[32] J. Yoshinobu, M. Kawai, J. Chem. Phys. 103 (1995) 3220.